J Appl Electrochem (2009) 39:71–81
DOI 10.1007/s10800-008-9642-z

ORIGINAL PAPER

Effects of electrolyte parameters on the iron/steel cathode potential in the chlorate process

Linda Nylén · Ann Cornell

Received: 12 March 2008 / Accepted: 10 July 2008 / Published online: 19 August 2008

Abstract This study focuses on how different electrolyte parameters of the chlorate process affect the cathode potential for hydrogen evolution on iron in a wide current-density range. The varied parameters were pH, temperature, mass transport conditions and the ionic concentrations of chloride, chlorate, chromate and hypochlorite. At lower current densities, where cathodic protection of the electrode material is important, the pH buffering capacity of the electrolyte influenced the potential to a large extent. It could be concluded that none of the electrolyte parameters had any major effects (<50 mV) on the chlorate-cathode potential at industrially relevant current densities (around 3 kA m^{-2}). Certainly, there is more voltage to gain from changing the cathode material than from modifying the electrolyte composition. This is exemplified by experiments on steel corroded from operation in a chlorate plant, which exhibits significantly higher activity for hydrogen evolution than polished steel or iron.

Keywords Chlorate cathode · Chlorate process · Hydrogen evolution · Iron · Steel

List of symbols

c_i	Concentration of species i (mol m^{-3})
D_i	Diffusion coefficient of species i (m^2 s^{-1})
E	Cathode potential vs reference electrode (Ag/AgCl) (V)
F	Faraday constant (As mol^{-1})
j_k	Current density for reaction k (A m^{-2})
k'_2	Coefficient in the Tafel expression of Eq. 2, which is given in Eq. 15 (mol m^{-2} s^{-1})
k_{14}	Coefficient in the Tafel expression of Eq. 14, which is given in equation 16 (m s^{-1})
N_i	Molar flux of species i (mol m^{-2} s^{-1})
R	Universal gas constant (J mol^{-1} K^{-1})
R_i	Homogeneous production rate of species i (mol m^{-3} s^{-1})
T	Temperature (K)
u_z	Convective velocity perpendicular to the electrode surface, i.e. in the direction of the z-axis (m s^{-1})
z	Axial coordinate (m)
α	Transfer coefficient
δ_D	Diffusion layer (m)
δ_R	Reaction layer (m)

1 Introduction

Sodium chlorate is produced from sodium chloride and water (Eq. 1) in un-divided electrochemical cells, in which hydrogen is evolved from reduction of water on the cathode and chloride is oxidised on the anode (Eqs. 2 and 3). Chlorine formed in the anodic reaction dissolves in the electrolyte and reacts with water through a number of steps, to eventually form the product sodium chlorate (Eqs. 4–6).

$$NaCl + 3H_2O \rightarrow NaClO_3 + 3H_2 \quad (1)$$

$$2H_2O + 2e^- \rightarrow H_2 + 2OH^- \quad (2)$$

$$2Cl^- \rightarrow Cl_2 + 2e^- \quad (3)$$

$$Cl_2 + H_2O \rightarrow ClOH + Cl^- + H^+ \quad (4)$$

L. Nylén (✉) · A. Cornell
Applied Electrochemistry, School of Chemical Science and Engineering, Royal Institute of Technology (KTH), SE-100 44 Stockholm, Sweden
e-mail: lindany@kth.se

$$ClOH \leftrightarrow ClO^- + H^+ \quad (5)$$

$$2ClOH + ClO^- \rightarrow ClO_3^- + 2H^+ + 2Cl^- \quad (6)$$

The addition of chromate to the chlorate electrolyte results in a cathodic current efficiency for hydrogen evolution of almost 100%, which otherwise would have been considerably lower due to side reactions such as reduction of hypochlorite and chlorate (Eqs. 7 and 8).

$$ClO^- + H_2O + 2e^- \rightarrow Cl^- + 2OH^- \quad (7)$$

$$ClO_3^- + 3H_2O + 6e^- \rightarrow Cl^- + 6OH^- \quad (8)$$

In the absence of chromate hypochlorite ions are easily reduced on iron (the major component in the most common steel electrodes), but the reaction becomes mass transport limited at higher current densities [1]. Reduction of chlorate is highly dependent on electrode material and does not take place to any major extent on Co, Ni, Mo, Ti, Hg and C, whereas iron oxides [2] and ruthenium dioxide [3] are active for chlorate reduction. In a previous study [1] the current efficiency for hydrogen evolution was determined for an iron cathode at 3 kA m^{-2} in a chromate-free electrolyte containing 550 g dm^{-3} $NaClO_3$ and 110 g dm^{-3} NaCl at 70 °C. The current efficiency was initially <50% and gradually increased over time to reach a value of >90% after 2 h of polarisation. Possibly iron oxides on the surface, catalysing chlorate reduction, had then been reduced.

When adding chromate to chlorate electrolyte a thin film of chromium hydroxide, $Cr(OH)_3 \bullet xH_2O$, forms on the cathode [4–6], see Eq. 9.

$$CrO_4^{2-} + 4H_2O + 3e^- \rightarrow Cr(OH)_3 + 5OH^- \quad (9)$$

The thin chromium-hydroxide film hinders its own growth as well as the parasitic reactions (Eqs. 7 and 8), while still allowing the hydrogen evolution to proceed on the cathode [5].

In the chlorate process electrical energy constitutes up to 70% of the production costs [7]. With the introduction of the dimensionally stable anode (DSA) in the 1970 s, the anode overpotential has decreased considerably and the highest overpotential is now connected to the steel cathode [8]. However, the widely used steel cathodes have the advantage of being fairly inexpensive and resistant to depositing impurities thanks to their surface renewal caused by corrosion during stops. Although the corrosion may be seen as a reactivation process it is of course disadvantageous in terms of consumption of the steel, which reduces the lifetime of the cathodes. Furthermore, the corrosion contaminates the electrolyte.

Extensive work has been carried out to decrease the overpotential by developing activated cathodes, most of them based on noble metals and titanium. Even though their catalytic activity towards hydrogen evolution has been satisfying they have not been industrially successful—probably not robust enough to survive in the industrial chlorate cell. Lately, higher costs for electricity have triggered intensified activity on the chlorate cathode potential, as shown by several recent patent applications. The approach has been to use electrocatalytic cathode coatings, containing ruthenium [9, 10] or electrodeposited Fe-Mo alloys [11, 12], as well as divided chlorate cells with coated cathodes [13] or gas diffusion electrodes [13, 14]. In the latter case hydrogen evolution has been replaced by the reduction of oxygen as cathode reaction, thereby cutting the cell potential substantially. Although the chlorate industry hopes to find a new depolarised cathode, the traditional steel cathode is still in use and is therefore the focus of this study. Most experiments in this study were made using an iron cathode, since iron is the major component in steel electrodes.

A typical chlorate electrolyte consists of 80–120 g dm^{-3} NaCl, 500–650 g dm^{-3} $NaClO_3$, 3–8 g dm^{-3} $Na_2Cr_2O_7$ and has a pH around 6–7 and a temperature of 70–80 °C. When varying these parameters, their effects on the whole process and on each other have to be taken into account. The electrolyte parameters are often interconnected and one parameter may have both positive and negative impacts. This is the case for the addition of chromate, which is necessary for keeping a high cathodic current efficiency, but is negative in terms of increased overpotential for both electrodes [1, 15, 16]. An additional positive effect of chromate is the enhanced buffer capacity in the pH range 5–7, where formation of chlorate (Eq. 6) has its highest rate. Chromate buffers according to Eqs. 10 and 11.

$$HCrO_4^- + OH^- \leftrightarrow CrO_4^{2-} + H_2O \quad (10)$$

$$HCrO_4^- \leftrightarrow CrO_4^{2-} + H^+ \quad (11)$$

To be able to separate the different effects of changing an electrolyte parameter, the influence on the anode and cathode reactions as well as on the homogeneous reactions has to be studied individually. In this study we have investigated the impact on the cathode potential.

In industrial cells, studies of varied electrolyte conditions are difficult to perform due to the interconnection between the different electrolyte parameters. The applied current density also has a strong impact on the electrolyte conditions. For instance, in industrial cells temperature and current density are strongly correlated, since heat is generated by the ohmic losses between the electrodes. Therefore, polarisation curves at constant temperature are almost impossible to measure for industrial cells. As a consequence, it is necessary to carry out complementary measurements in lab cells, for which a single parameter can be varied while holding the others relatively constant.

Variations of electricity tariffs during the hours of the day in combination with the increasing prices may force the chlorate plants to operate at varying current loads. When electricity prices peak it may be advantageous to minimise the production rate. However, at low currents it has to be assured that that the steel is under cathodic protection to avoid corrosion. According to Coleman and Tilak [17] this value of the cathodic current density is approximately 15–75 A m^{-2}, depending on cell conditions. The demand for operation at varying current loads requires knowledge about how the cathode behaves in a wide current-density range.

In the literature most studies regarding chlorate-electrolyte conditions concentrate on investigating the current efficiency, see e.g. Ref. [2, 18–24], and a few focus on the DSA-anode potential [15, 16, 25–27]. For the steel and iron cathodes, polarisation curves at chlorate-like conditions are scarcely presented [1, 28, 29]. Dobrov and Elina measured polarisation curves on steel in chlorate electrolyte at varied chromate concentration [29] and to our knowledge no work besides that has been published on the effect of different electrolyte parameters on the cathode potential. Some of these parameters affect hydrogen evolution in general, irrespective of the electrode material, and may be important to consider in the development of new cathode concepts.

The aim of this study was to investigate how different chlorate-electrolyte parameters impact the cathode potential for hydrogen evolution in a wide current-density range by recording iR-corrected polarisation curves on rotating disk electrodes (RDE) of iron and steel. The parameters varied were pH, temperature, mass transport conditions and the ionic concentrations of chloride, chlorate and chromate as well as the addition of hypochlorite ions. The current-density range for the polarisation curve was 10 A m^{-2}–3 kA m^{-2}. In addition to the experimental work, modelling work aiming at investigating the effect of chromate buffering in the cathodic diffusion layer was carried out.

2 Experimental

All polarisation curves were made in a three-electrode jacketed glass cell, connected to a water bath for temperature control. The working electrode was either an RDE or a rotating cylinder electrode (RCE) mounted on an electrode rotator, model 636 from EG&G. A large area platinum mesh was employed as counter electrode. The reference electrode was an Ag/AgCl electrode (K201 from Radiometer, +0.197 V vs NHE) with saturated KCl at room temperature connected to a Luggin capillary by a salt bridge, containing 5 M NaCl or 3 M $NaClO_3$ (for chloride-free measurements).

2.1 Electrolyte

The "standard" chlorate electrolyte contained 550 g dm^{-3} $NaClO_3$ (Eka Chemicals), 110 g dm^{-3} NaCl (p.a. grade) and 3 g dm^{-3} $Na_2Cr_2O_7$ (p.a. grade) with no added NaClO at 70 ± 1 °C. Water purified in a Millipore system was used in all experiments. Any deviations from these conditions are given in the text.

The pH was adjusted with 5 M HCl and 5 M NaOH, except in the chloride-free case where $HClO_4$ and NaOH were used. In case NaClO was added, it was added from a concentrated solution from BDH Laboratory Supplies. After addition, the initial concentration of the electrolyte was 1 g dm^{-3} NaClO, but decreased with time as ClO^- formed chlorate.

2.2 Electrodes

To imitate industrial conditions, studies of the chlorate cathode should preferably be made with industrially operated electrodes, which have a complex surface composition of oxides as well as deposited impurities. However, experiments involving industrially corroded electrodes lead to unsatisfactory reproducibility, since an electrode cannot be used for more than one polarisation curve, as the composition of the electrode surface changes during the experiment. Therefore, most experiments in this work have been made using an iron electrode, since iron is the major component in the industrial steel cathodes and a good reproducibility could be achieved by polishing the electrode surface prior to the experiment. These results have been compared to polarisation curves on samples cut from steel cathodes that had been in industrial operation.

The iron RDE consisted of an iron disc (diameter 5 mm, specpure from Johnson Matthey) embedded in a Teflon sheath. Prior to every polarisation measurement it was polished with 4000 grade silicon-carbide grinding paper, and thereafter thoroughly rinsed with Milli-Q water.

Steel RDEs (low carbon steel grade with iron content >99%) of 1 cm^2 were punched from cathode plates (either new or operated in the chlorate process) and placed into titanium holders suitable for the electrode rotator. Bare titanium was masked with silicon tubing and epoxy to hinder electrochemical reactions taking place on the holder. New, non-corroded steel electrodes were polished with 4000 grade silicon-carbide grinding paper before being put into the holders. To remove oxides formed in the time between silicon-carbide polishing and measurement the electrode surface was gently polished with alumina paste (Alpha micropolish alumina No.1C with particle size 1.0 μ from Buehler) and washed with acetone in an ultrasonic bath, followed by water (milli-Q) rinsing just before the experiment. Corroded steel electrodes had been

operated in a chlorate plant and washed with water only, thus having traces of chromium, calcium etc. deposits on the corroded surface.

For measurements at low mass-transport conditions a RCE of iron (12 mm diameter, 3 cm^2, made from 99.99% iron from Alfa Aesar) was used. Prior to measurements the electrode was polished with alumina paste and rinsed as described above.

2.3 Measurements

The electrodes were submerged into the electrolyte under cathodic galvanostatic control at 10 kA m^{-2} to assure a vigorous hydrogen evolution on the electrode, thus avoiding oxidation of the surface. To obtain a high cathodic current efficiency for hydrogen evolution, the electrodes were pre-polarised in order to form a chromium film at the surface. On a newly polished electrode the film is formed almost instantly [1] and only a short pre-polarisation of 2 min (10 kA m^{-2}) before recording a polarisation curve was considered necessary. The corroded electrodes needed longer pre-polarisation to reach a high current efficiency [22] and they were therefore operated at 10 kA m^{-2}, at 3,000 rpm, for 1 h in a separate chlorate solution. To retain the chromate film, the electrodes were removed from the pre-polarisation electrolyte still under galvanostatic control, and were thereafter rinsed with water to remove electrolyte traces that otherwise could have caused film dissolution. When submerged in the new chlorate electrolyte the electrodes were under galvanostatic control and were operated at 10 kA m^{-2} for 2 min in order to obtain a stable potential before starting the polarisation measurements.

Galvanostatic polarisation curves were recorded using a PAR273A potentiostat, with the current decreasing stepwise from high to low current densities. Correction for iR-drop was made using a current interrupt technique [15]. By starting the measurements at high cathodic current densities and from there decreasing the current, oxidation of the electrode surface was avoided. Some corrosion may occur at low current densities, however, there were no visible signs of corrosion products on an electrode surface after it had been subjected to a polarisation-curve measurement.

For each experiment, five consecutive polarisation curves were recorded, with electrolyte pH adjusted and the electrode polished prior to each measurement. To illustrate the reproducibility of the measurements error bars are shown in the polarisation curves of Fig. 2. The best reproducibility was achieved when using the pure iron RDE, since this electrode could be polished with silicon-carbide grinding paper prior to each experiment. For these experiments the maximum variation of the polarisation curve ranged between ±4 and ±10 mV, in the current range 3 × 10^2–3 × 10^3 A m^{-2}. Polishing with alumina paste, as for the RCE, resulted in slightly larger variation, ±10 to ±15 mV, in the same current range. The corroded steel electrodes could only be used once, since their surface composition changed during the experiment as the oxides were reduced. Therefore, in Fig. 9 only the first recorded curve of each polarisation experiment is shown. Also the curve with hypochlorite added (Fig. 3) is the first recorded curve since as time passed the hypochlorite reacted to chlorate and its concentration decreased. All other polarisation curves of this paper are average values of five measurements.

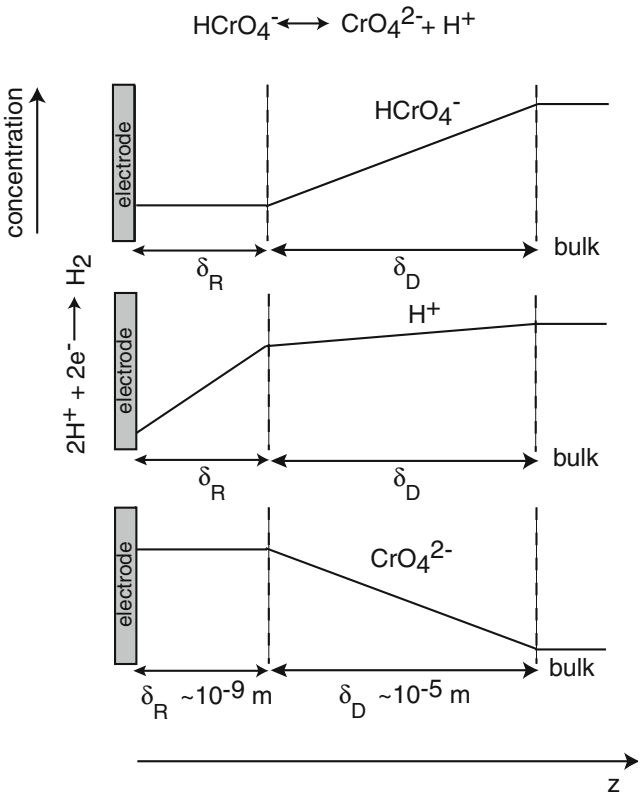

Fig. 1 Schematic concentration profiles for a system, in which with a chemical reaction ($HCrO_4^- \rightarrow CrO_4^{2-} + H^+$) precedes the electrode reaction ($2H^+ + 2e^- \rightarrow H_2$). $HCrO_4^-$ diffuses towards the electrode surface (through the diffusion layer, δ_D). Close to the cathode, in the reaction layer (δ_R), the chemical reaction produces H^+ to the electrode reaction. The thickness of the diffusion layer is in the order of 10^{-5} m, while the reaction-layer thickness is in the order of 10^{-9} m

3 Model

The model of this work takes into account the complex interplay between the pH-raising electrode reactions for hydrogen evolution, mass transport and homogeneous reactions. It predicts the cathodic polarisation curves and gives information about the approximate reaction rates and the nature of the chromate buffering reaction. The model is

one-dimensional and is based on a previously developed model [30], where oxygen evolution on a RDE in a chromate-buffered solution was simulated and where it was found that the important part of the buffering took place in a very thin reaction layer (in the order of nanometers) at the anode by CrO_4^{2-} and H_2O forming $HCrO_4^-$ and OH^- (Eq. 10). The oxygen-evolving system of the original model is analogous to the system of this work, with a polarisation curve of two regions, one pH-dependent at low current densities and one pH-independent at higher current densities. Consequently, the thin reaction layer due to chromate buffering was therefore also expected to appear in the simulations of the hydrogen-evolving cathode of this work.

A reaction layer may develop in systems in which a chemical step (in this case the buffering reaction) precedes the electron transfer. The reaction layer theory is described by Albery [31], and is illustrated in Fig. 1 by schematic concentration profiles for the system of this work. A simplified example is used for the illustration, with the electrode reaction being proton reduction in combination with homogeneous chromate buffering due to Eq. 11. When the $HCrO_4^-$ ions are close enough to the electrode surface the H^+ ions produced by the buffering reaction (Eq. 11) diffuse to the electrode surface faster than they may recombine with CrO_4^{2-}. Within the diffusion layer equilibrium between the different species prevails, while in the reaction layer H^+, CrO_4^{2-} and $HCrO_4^-$ are in disequilibrium. The reaction layer thickness is very thin compared to the diffusion layer. To capture the steep gradient of H^+ in the reaction layer it is important to have a good resolution of the region close to the electrode surface. The concentration profiles of the picture would be affected by e.g. reaction rates, current density, electrode rotation rate, additional homogeneous and electrode reactions, etc.

The model is based on mass balances at steady-state for each species i in the electrolyte:

$$-\frac{\partial N_i}{\partial z} + R_i = 0 \tag{12}$$

where N_i is the molar flux and R_i is the production rate of species i by homogeneous reactions. Due to the high ionic strength of the electrolyte (approximately 5 M $NaClO_3$ + 2 M NaCl), transport by migration of minority species like H^+, OH^- and chromate species could be neglected. Reducing the model, by assuming transport only by convection and diffusion, allowed the time for calculation to be shortened considerably. Simulations including migration and simulations in which migration was neglected gave almost identical results. The molar flux, N_i, of specie i is expressed by the Nernst-Planck equation, with the migration term neglected (Eq. 13).

$$N_i = u_z c_i - D_i \frac{\partial c_i}{\partial z} \tag{13}$$

In the equation above u_z is the convective velocity, in the direction perpendicular to the disk surface, D_i is the diffusion coefficient and $\partial c_i/\partial z$ is the concentration gradient of specie i. The potential and concentration-dependent electrode reactions are used as boundary conditions and in the bulk electrolyte all concentration gradients are assumed to be zero. The species solved for were H^+ and OH^-, CrO_4^{2-} and $HCrO_4^-$. The buffering effect of hypochlorite was not included in the simulations, since focus of the model was to capture the buffer effect of chromate; by this the complexity of the model was reduced. In the experiments, to which the simulation results were compared, no hypochlorite was added to the electrolyte and no significant amounts were built up during the short time of the experiment.

For the oxygen-evolving model developed previously [30], the electrode reactions were oxygen evolved from OH^- and oxygen evolved from water. These electrode reactions are in this work replaced by hydrogen evolved from H^+ (Eq. 14) and hydrogen evolved from water (Eq. 2). The currents, j_2 and j_{14} were assumed to follow Tafel expressions, whose parameters were derived from data taken from the experimental polarisation curve at pH 6.5 in Fig. 2 (similarly as in the previous study [30]). Since the model required Tafel parameters as input data, slopes had to be estimated although they change continuously throughout the polarisation curve. The slopes are approximate values and are extracted at both sides of the limiting current, i.e. at lower current densities for H^+ reduction and at higher for water reduction. However, the focus of the

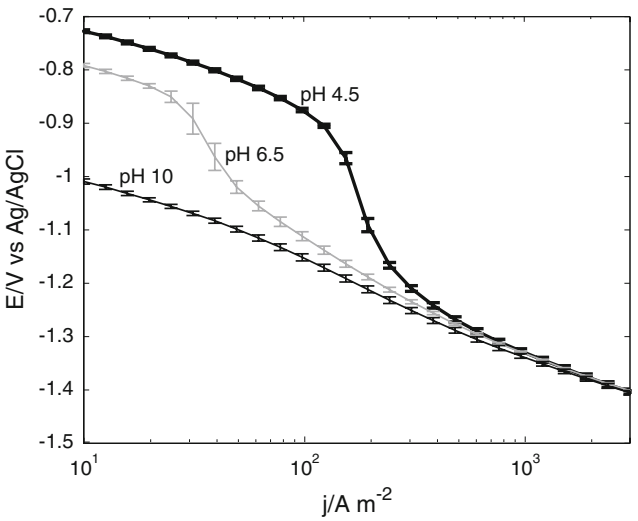

Fig. 2 Polarisation curves on a pure iron RDE in chlorate electrolyte (550 g dm^{-3} $NaClO_3$, 110 g dm^{-3} NaCl, 3 g dm^{-3} $Na_2Cr_2O_7$) at pH 4.5, 6.5 and 10, 70 °C, rotation rate 3,000 rpm

model is to capture the buffer effect of chromate on the limiting current of H^+ reduction, which is almost unaffected by the slopes.

$$2H^+ + 2e^- \rightarrow H_2 \quad (14)$$

The currents for the hydrogen-evolving Eqs. 2 and 14, were expressed as

$$j_2 = Fk_2' \exp\left\{\frac{-\alpha_2 FE}{RT}\right\} \quad (15)$$

$$j_{14} = Fc_{H^+}k_{14} \exp\left\{\frac{-\alpha_{14} FE}{RT}\right\} \quad (16)$$

where k_2', since water is in excess, may be seen as a concentration–independent rate constant for Eq. 2. Therefore, j_2 has no concentration dependence either. The transfer coefficients are α_2 and α_{14}, E is the cathode potential, T the temperature, F Faraday's constant, c_{H+} the concentration of H^+ at the cathode surface and k_{14} is the cathodic rate constant for Eq. 14. The reaction order with respect to H^+ was assumed to be one. The values of the kinetic parameters were k_2' (mol s^{-1} m^{-2}) = 3.5 × 10^{-10}, k_{14} (s^{-1} m) = 8.1 × 10^{-8}, $\alpha_2 = 0.4$, $\alpha_{14} = 0.6$.

The homogeneous reactions taken into account in this work were water dissociation ($H^+ + OH^- \leftrightarrow H_2O$) and chromate buffering (Eq. 10 or 11).

The Convective-Diffusion mode of Comsol Multiphysics was used for solving the equation system.

4 Results and discussion

When discussing the results of this study a decreasing potential means the potential going to more negative values, thus resulting in an increased cell potential and higher energy consumption. High cathode potential (less negative potential) is desired in order to minimise the energy cost.

4.1 Electrolyte pH

Figure 2 shows the effect of pH on the cathodic polarisation curve for an iron electrode in chlorate electrolyte. The error bars indicate the reproducibility in each point, based on five consecutively measured polarisation curves (each with a newly polished electrode and pH adjusted). An apparent pH dependency is seen at lower current densities (<3 × 10^2 A m^{-2}), but as the current density is increased the polarisation curves for the different pHs coincide and at industrial full-load current densities (around 3 kA m^{-2}) the potential is not affected by the electrolyte pH. This pH independence is due to the electrode reaction being reduction of water (Eq. 2), which at high overpotentials is a pH-independent reaction [32]. The pH effect at lower current densities (<3 × 10^2 A m^{-2}) is explained by the dominating reaction for pH at both 4.5 and 6.5 being H^+ reduction (Eq. 14) [32]. When the pH is sufficiently low (pH 4.5 and 6.5 in Fig. 2) hydrogen evolution from H^+ (Eq. 14) is kinetically favoured, although it suffers from poor supply of H^+ ions at higher current densities. The poor supply is seen in Fig. 2 as a transition region of high slopes connecting the pH dependent region with the pH independent one (for pH 4.5 at around 3 × 10^2 A m^{-2} and for pH 6.5 at around 4 × 10^1 A m^{-2}). This transition region is here defined as a limiting current for hydrogen evolution from H^+. The limiting current is dependent on pH and is not visible at low H^+ concentrations, as for pH 10, where hydrogen is only evolved from water (Eq. 2).

4.2 Chromate and hypochlorite addition

Figure 3 illustrates the impact of chromate and hypochlorite on the cathodic polarisation curve of iron in chlorate electrolyte. The most evident effect of an increased chromate concentration is seen at −0.85 to −1.1 V, where the limiting current, due to poor supply of H^+, appears. This may be related to the buffering properties of chromate. At current densities higher than the limiting current the consequence of increasing the chromate content from 3 g dm^{-3} $Na_2Cr_2O_7$ to 9 g dm^{-3} is only a minor decrease in cathodic potential (less than 20 mV). The chromate film has been shown to increase in thickness with increasing chromate concentration in the electrolyte [33], which may impact the rate of hydrogen evolution.

Hypochlorite added to the electrolyte affects the potential in the whole current range of Fig. 3. At current densities lower than approximately 10^2 A m^{-2} presence of

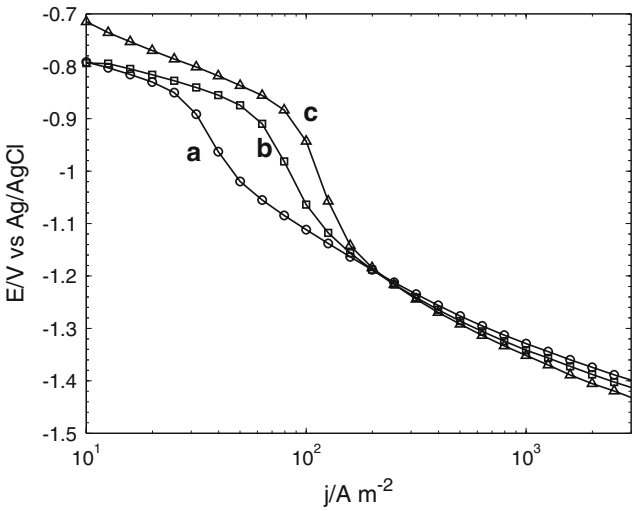

Fig. 3 Polarisation curves on a pure iron RDE in chlorate electrolyte (550 g dm^{-3} $NaClO_3$, 110 g dm^{-3} NaCl)) at pH 6.5, 70 °C, rotation rate 3,000 rpm, with (a) 3 g dm^{-3} $Na_2Cr_2O_7$, (b) 9 g dm^{-3} $Na_2Cr_2O_7$, (c) 3 g dm^{-3} $Na_2Cr_2O_7$ and approximately 1 g dm^{-3} NaClO

hypochlorite increases the cathode potential. This is possibly due to the chromate film not hindering hypochlorite reduction fully. Hypochlorite reduction is limited by mass transport at higher current densities, and the increase in limiting current seen in Fig. 3 may be a mixed limiting current due to both limited supply of H^+ and transport-limited hypochlorite. Similar to chromate, hypochlorite acts as a buffer through Eq. 5 which would supply H^+ to the hydrogen evolution reaction and increase the limiting current for Eq. 14. Surprisingly, at industrial full-load current densities (around 3 kA m^{-2}) Fig. 3 shows that addition of hypochlorite has a negative effect on the cathode potential of about 20 mV.

The impact of chromate buffer on the limiting current for hydrogen evolution from H^+ is evident in Fig. 3. The increase in limiting current may be explained by the buffer serving as a source of H^+, thereby decreasing the pH-raising effect of the hydrogen-evolving reaction. Hurlen et al. [32] have studied how hydrogen evolution on iron in chloride electrolyte is influenced by different amounts of added acetate buffer. They saw a clear relation between increased acetate content and an increased limiting current for hydrogen evolution from H^+. This is consistent with the increase due to addition of chromate buffer in this study.

Figure 2 as well as Fig. 3 shows convincing signs for the polarisation curve being built up of two different reactions for hydrogen evolution (H_2 from H^+ and H_2 from H_2O) connected by a limiting current due to poor H^+ supply; a simulation of the system provides further evidence for this. Additionally, such a model gives information about the approximate reaction rates and the nature of the chromate buffering reaction. In Fig. 4, modelled polarisation curves for two different chromate concentrations are presented and

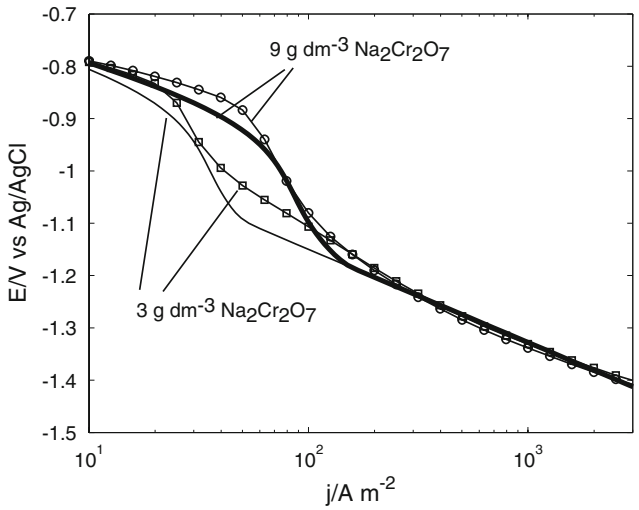

Fig. 4 Experimental polarisation curves in chlorate electrolyte at pH 6.5 (lines with symbols) and simulated polarisation curves (solid lines): 3 g dm^{-3} $Na_2Cr_2O_7$ and 9 g dm^{-3} $Na_2Cr_2O_7$, 3,000 rpm, 70 °C

compared with the experimental ones. For the oxygen-evolving system the buffering was previously shown to proceed through $HCrO_4^- + OH^- \rightarrow CrO_4^{2-} + H_2O$ (Eq. 10) [30], but using the same reaction in the model for hydrogen evolution resulted in disagreement between experiments and simulations, with the simulated limiting current for hydrogen evolution from H^+ being too low. Increasing the reaction rate of the buffering reaction did not affect the polarisation curve, since in this case the limiting factor was the dissociation rate of water, and the simulated current would only become higher by speeding up the water dissociation to unrealistic values. Therefore, the reaction $HCrO_4^- \leftrightarrow CrO_4^{2-} + H^+$ (Eq. 11) was proposed to be responsible for increasing the limiting current of hydrogen evolution from H^+ at the iron cathode. The rate of the reaction was expressed as $k_f \cdot c_{HCrO_4^-} - k_b \cdot c_{CrO_4^{2-}} \cdot c_{H^+}$, and the reaction rate constants were estimated by comparing the simulated limiting current of H^+ reduction (Eq. 14) with the experimental one. In the presented curves, the kinetic parameter values of Eq. 11 are $k_f = 1 \times 10^5$ [s^{-1}] and $k_b = 7.9 \times 10^7$ [m^3 mol^{-1} s^{-1}]. For 3 g dm^{-3} $Na_2Cr_2O_7$ as well as for 9 g dm^{-3} a good agreement between experiments and simulations is seen, when modelling the chromate buffering as Eq. 11. Most likely, chromate buffers by both Eqs. 10 and 11, but only Eq. 11 has an effect on the polarisation curve for hydrogen evolution from H^+. Similarly to anodic oxygen evolution in chromate-containing electrolyte [30], the buffering for the hydrogen-evolving system takes place in a very thin reaction layer (in the order of nanometers) close to the cathode surface. This reaction layer is indicated by a very steep concentration profile for H^+, arising when H^+ produced from the buffering (Eq. 11) diffuses to the cathode surface faster that it recombines with CrO_4^{2-}. The concentration profiles were found to be similar to the expected ones, shown in the schematic illustration in Fig. 1.

4.3 Chloride and chlorate concentrations

On the chlorate anode high concentrations of sodium chlorate (>600 g dm^{-3}) increase the potential at high current densities (>3 × 10^3 A m^{-2}) [27]. To investigate whether a similar effect of increased ionic strength could appear at the cathode, the sodium chlorate concentration was varied between 450 g dm^{-3} and 650 g dm^{-3}, keeping the sodium chloride concentration constant at 110 g dm^{-3}. In Fig. 5a, b the results are displayed, which show that, similarly to the anode, the increase in chlorate concentration has a negative effect on the cathode potential. At the current densities where hydrogen evolution from water (Eq. 2) is dominating (around 5 × 10^1–3 × 10^3 A m^{-2}) an increase of the sodium chlorate concentration from 450 to 650 g dm^{-3} gives around 30 mV decrease in cathodic potential. Figure 5a, b also displays the polarisation curves recorded in pure 5 M

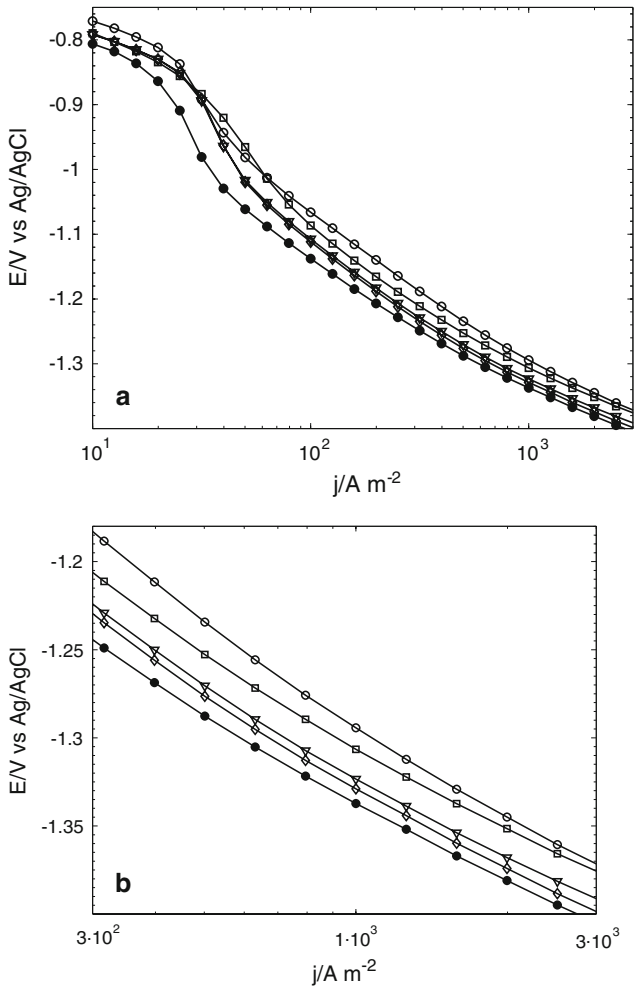

Fig. 5 **a** and **b** (zoom of Fig. 5a). Polarisation curves on a pure iron RDE in electrolytes of varied composition. Temperature 70 °C, pH 6.5, 3 g dm^{-3} $Na_2Cr_2O_7$, rotation rate 3,000 rpm; (○) 5 M (292 g dm^{-3}) $NaClO_3$, (□) 5 M (532 g dm^{-3}) NaCl, (▽) 450 g dm^{-3} $NaClO_3$ and 110 g dm^{-3} NaCl, (◇) 550 g dm^{-3} $NaClO_3$ and 110 g dm^{-3} NaCl, (●) 650 g dm^{-3} $NaClO_3$ and 110 g dm^{-3} NaCl

(292 g dm^{-3}) NaCl electrolyte and in 5 M (532 g dm^{-3}) $NaClO_3$ electrolyte. The chloride solution gives a slightly lower cathode potential for water reduction by approximately 10-30 mV compared to the pure chlorate electrolyte. This result may be compared with the results of Vračar and Dražić, which showed an increased overpotential for hydrogen evolution when chloride ions were added to an electrolyte of sulphuric acid [34]. The authors explained this as an effect of chloride ions adsorbing to the iron surface and affecting the reaction kinetics for hydrogen evolution, possibly by blocking the hydrogen-evolving sites.

4.4 Mass transport

Figure 6 shows the effect of mass transport on the polarisation curve of an iron electrode in chlorate electrolyte.

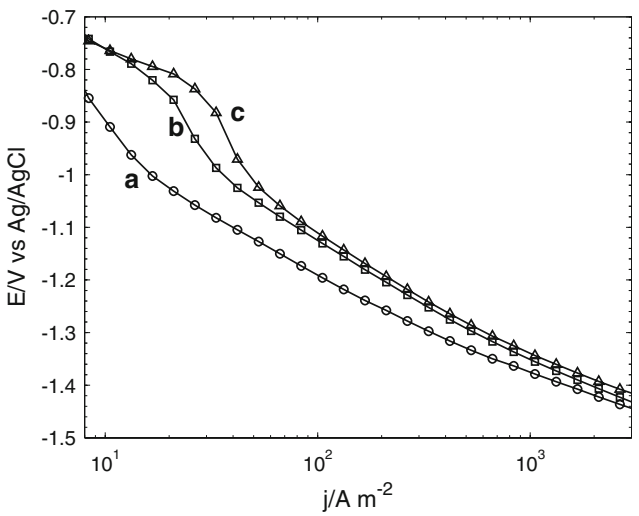

Fig. 6 Polarisation curves on a rotating cylinder iron electrode in chlorate electrolyte (550 g dm^{-3} $NaClO_3$, 110 g dm^{-3} NaCl, 3 g dm^{-3} $Na_2Cr_2O_7$) at pH 6.5 and 70 °C. Rotation rate (a) 200 rpm, (b) 1,000 rpm, (c) 2,000 rpm

The electrode was a rotating cylinder, allowing gas bubbles to rise freely from the surface instead of being trapped beneath the electrode as for the rotating disk at low rotation rates. As expected, an increasing rotation rate increases the limiting current for hydrogen evolution from H^+ (Eq. 14). However, even in the region where hydrogen evolution from reduction of water is the dominating reaction (approximately $>10^2$ A m^{-2}) a low rotation rate affects the polarisation curve by decreasing the cathode potential. This might be due to slow transport of gas bubbles produced at the electrode, leading to a reduction in surface area available for reaction. An increase in rotation rate from 1,000 to 2,000 rpm did not cause any significant changes in potential in the region where hydrogen is produced from water molecules (approximately $>10^2$ A m^{-2}).

To be able to apply the results from the RDE measurements and simulations to industrial conditions, the difference in mass transport between the different cells has to be taken into account. The RDE acts like a pump, dragging electrolyte towards its surface, while the mass transport in a chlorate cell is induced by the hydrogen gas bubbles rising upwards through the cell gap, between the parallel electrode plates. One approach is to compare the diffusion layer thickness of the modelled RDE with the one of a simulated industrial cell. Byrne et al. [35] simulated a chlorate cell and calculated the concentration profiles of chloride at the anode for a current density of 2.5 kA m^{-2} and an inlet flow rate of 0.75 m s^{-1}, which was considered typical for an industrial cell. The diffusion layer thickness varied along the height of the cell, and was zero at the bottom where fresh electrolyte enters and around 120 μm at the top. Halfway up the cell height the diffusion layer

thickness was around 60 μm. The simulations of this work showed that this thickness corresponds to that of a rotation rate of 300 rpm for the rotating disk. Comparing the simulated limiting current density for a rotation rate of 3,000 rpm (the rotation rate used in the RDE experiments) with that for 300 rpm, gives a limiting current density which is approximately 40% less for 300 rpm. However, at such a low rotation rate the RDE measurements could not be carried out at technical current densities, since hydrogen gas bubbles accumulated at the electrode surface.

4.5 Temperature

In Fig. 7 polarisation curves on iron in chlorate electrolyte at four different temperatures are displayed. At low current densities where hydrogen is evolved from H^+ reduction ($<3 \times 10^1$ A m^{-2}) the temperature has a minor influence on the potential. In the current density region where industrial cells are operated at full load (around 3 kA m^{-2}) and hydrogen is evolved through water reduction, the cathode potential became less negative with higher temperature. This behaviour is expected since a higher temperature increases the reaction rate. Figure 8 shows that for a current density of 1 kA m^{-2} the potential is increased approximately linearly with 1.9 mV/°C, while for 3 kA m^{-2} the potential increases with 1.6 mV/°C. For the chlorate process 70–80 °C is considered to be the optimum temperature [18], since both lower and higher temperatures would increase the oxygen-forming side reactions (oxygen is evolved either electrochemically on the anode or by homogeneous decomposition of ClO^- or ClOH in the bulk). Tilak and Chen [18] proposed that a higher temperature would not only increase the rate of the electrode reactions,

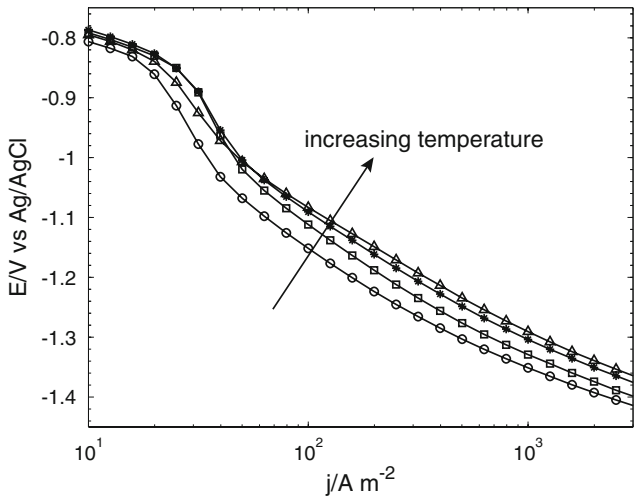

Fig. 7 Polarisation curves on a pure iron RDE in chlorate electrolyte (550 g dm^{-3} $NaClO_3$, 110 g dm^{-3} NaCl, 3 g dm^{-3} $Na_2Cr_2O_7$) at pH 6.5, rotation rate 3,000 rpm; (○) 61 °C, (□) 70 °C, (■) 83 °C, (Δ) 92 °C

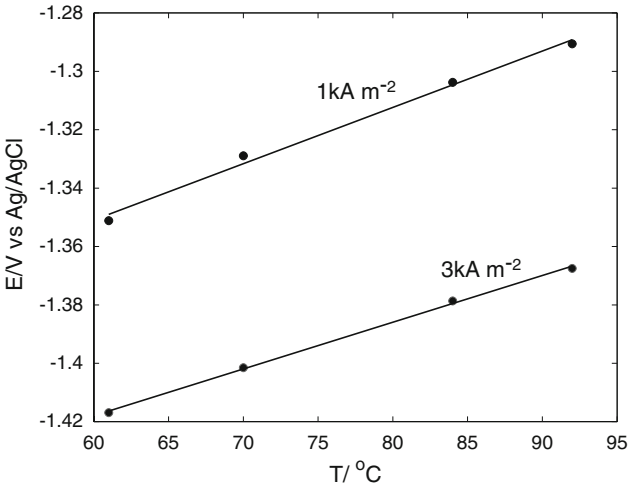

Fig. 8 Cathode potential as function of electrolyte temperature. The slope for 1 kA m^{-2} is 2 mV °C^{-1} and for 3 kA m^{-2} 1.6 mV °C^{-1}. (Data taken from Fig. 6)

but also increase the rate of the oxygen-forming side reactions, while a lower temperature would decrease the rate of chlorate formation through Eq. 6 and high concentrations of hypochlorite and hypochlorous acid would be built up through Eqs. 4 and 5. The hypochlorous acid and the hypochlorite would then react to form oxygen. It was previously shown that the potential for chloride oxidation on the anode (Eq. 3) decreases with increased temperature by 1 mV/°C at 1 kA m^{-2} and by 2 mV/°C at 3 kA m^{-2} [16]. Increasing the temperature by 10 °C at 3 kA m^{-2} would consequently lower the total cell potential by at least 35 mV, which corresponds to approximately 1% of the cell potential (normally around 3 V), and would of course affect the iR-losses as well. Even though this figure might seem small it would reduce the energy consumption significantly, due to the large production volumes of chlorate. The apparent activation enthalpy, ΔH_c, for the hydrogen evolution was derived from the polarisation curves in Fig. 7 according to the method described by Koryta and Dvorák in [36] (also used in Ref. [16]). It involves plotting log(i) vs $1/T$ at constant potential; the apparent activation enthalpies may be derived from the slope of the curve. We found apparent activation enthalpies of 24–30 kJ mol^{-1} at −1.2–(−1.4) V versus Ag/AgCl. These values are slightly lower than those found by Tamm et al. [37]. The latter made their experiments of hydrogen evolution on iron in sulphuric acid at 5–25 °C and calculated activation enthalpies of approximately 35–45 kJ mol^{-1}.

4.6 Steel electrodes

In Fig. 9 polarisation curves in chlorate electrolyte on corroded and non-corroded steel electrodes punched from industrial cathode plates are compared with the polarisation

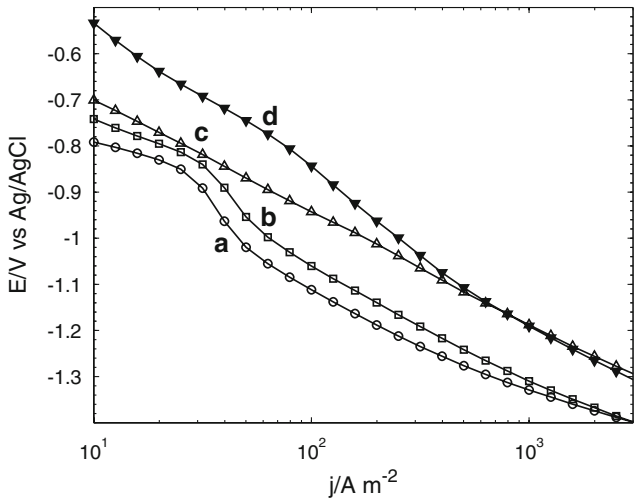

Fig. 9 Polarisation curves in chlorate electrolyte (550 g dm^{-3} $NaClO_3$, 110 g dm^{-3} NaCl, 3 g dm^{-3} $Na_2Cr_2O_7$), 70 °C, rotation rate 3,000 rpm; (a) pure iron RDE, pH 6.5, (b) polished steel RDE, pH 6.5, (c) corroded steel RDE, pH 6.5, (d) corroded steel RDE, pH 4.5

curve on pure iron. The non-corroded steel electrode had only been gently polished prior to the measurements (the titanium holder did not allow polishing with silicon-carbide grinding paper) and consequently there could be oxides on the surface. Still, the pure iron electrode behaved similarly to the non-corroded steel electrode, which validates the use of pure iron as model material for industrial steel cathodes.

As mentioned in the introduction, the cathodes in industry have electrolyte impurities precipitated on the surface and are usually corroded after having lost their cathodic protection during stops. These are factors that influence the catalytic activity of the electrode. The corroded steel electrodes in Fig. 9 had been operated in a chlorate plant and then washed with water before being used in the measurements of this study. Compared to the non-corroded steel electrode, the corroded steel surface is more active towards HER, in particular in the high current density region (>50 A m^{-2}) where the overpotential is approximately 100 mV lower. This may be compared with results from an earlier study of this group [1], in which an iron electrode, corroded in chlorate electrolyte, obtained a lowered potential for hydrogen evolution compared to the non-corroded iron. Cornell et al. compared polarisation curves for iron electrodes corroded at open circuit with non-corroded iron electrodes. The apparent increase in activity for hydrogen evolution at the corroded electrodes could be due to a catalysing effect of oxides or an increase in surface area, but in the light of later results [22], the apparent activation effect [1] may also be due to reduction of chlorate. The activity for this side reaction is favoured by the presence of oxides on iron electrodes [1, 2] and the chromate film has to be built up properly to avoid confusion between increased activity for hydrogen evolution and an increased current due to side reactions. On corroded steel electrodes a high current efficiency for hydrogen evolution was not achieved immediately, but needed around 1 hour of cathodic polarisation in chlorate electrolyte with 3 g dm^{-3} $Na_2Cr_2O_7$ at 3 k Am^{-2} to reach a constant level of around 95% [22]. Therefore, the industrially corroded electrodes were given a protecting chromate film at constant current density for 1 h in chromate-containing chlorate electrolyte.

Two polarisation curves were recorded for the corroded steel electrodes, one at pH 4.5 and another at pH 6.5. For pH 6.5 (industrial pH) a single reaction seems to dominate, since an almost constant slope is found for the whole current range. Increasing the H^+ concentration by lowering the pH to 4.5 resulted in an increased potential at lower current densities (<2 × 10^2 A m^{-2}), whereas at higher current densities (>5 × 10^2 A m^{-2}) the curve coincides with the curve for pH 6.5. This indicates that for pH 6.5 the single reaction is hydrogen evolved from water (Eq. 2), while for pH 4.5 the two different reactions for hydrogen evolution (hydrogen formed from H^+ and from water) may be distinguished. It appears as if the corroded surface activates the reduction of water (Eq. 2) more than the reduction of H^+ (Eq. 14). Alternatively, H^+ reduction might be somewhat suppressed on the corroded surface and the higher activity displayed for water reduction could also be an effect of increased surface area due to corrosion. Further work is needed to investigate the contribution of increased surface area and the catalytic effect of the various corrosion products.

5 Conclusions

In this work the impact of several electrolyte parameters (pH, temperature, mass transport, the concentrations of chloride, chromate and chlorate as well as the presence of hypochlorite) on hydrogen evolution during chlorate electrolysis has been experimentally investigated. The electrode material used was mainly iron, since it is the major component in industrial steel cathodes. These results have been compared with measurements on electrodes made from polished and industrially corroded steel cathodes. Additionally, the effect of chromate buffering on hydrogen evolution has been studied by simulating mass transport and homogeneous reactions with the potential and concentration-dependent electrode reactions as boundary conditions.

At low current densities, where H^+ reduction on iron and steel reached a limiting current, the pH buffering capacity associated with chromate and hypochlorite influenced the potential significantly. On the corroded steel electrode, in pH 6.5 electrolyte, no H^+ reduction appeared to take place and hydrogen evolved through water reduction.

Consequently, the large potential step at the limiting current for H^+ reduction would not have to be taken into particular consideration when using corroded steel electrodes. This may however be important for other cathode materials when electricity prices are high and the process is occasionally operated at lower loads. The buffering capacity of the electrolyte species must be considered when operating close to the limiting current, since even a small current change may, by the large potential step, move the potential into a range where the cathodic protection may be lost.

It could be concluded that none of the electrolyte parameters had any major effects on the chlorate-cathode potential at industrial full-load current densities (around 3 kA m^{-2}), where water reduction was dominating. Although the electrolyte conditions were varied to unrealistic values their impact was never larger than 50 mV, mostly significantly smaller.

Certainly, there is more voltage to gain from changing the cathode material and/or structure than from modifying the electrolyte composition. This is indicated when comparing the results of this study with polarisation measurements on cathodes containing ruthenium, showing considerably lowered overpotentials [3, 38]. The importance of the electrode is further shown by the experiments on steel corroded from operation in a chlorate plant, which exhibits significantly higher activity for hydrogen evolution than polished steel or iron. It is likely that the composition at the corroded electrode surface activates the cathode reaction and decreases the overpotential, probably in combination with an increased surface area of the electrode.

Modelling results showed that the most likely reaction for the chromate buffering in the investigated system was $HCrO_4^- \leftrightarrow CrO_4^{2-} + H^+$, rather than $HCrO_4^- + OH^- \leftrightarrow CrO_4^{2-} + H_2O$. However, both reactions may buffer even though only one has an impact on the cathodic polarisation curve. In future modelling of the chlorate cell it has to be taken into account that equilibrium of chromate buffering cannot be assumed at the electrodes and therefore the rate constants of the reactions as well as their nature become important.

Acknowledgements This work was financed by the Swedish Energy Agency, Eka Chemicals AB and Permascand AB.

References

1. Cornell A, Lindbergh G, Simonsson D (1992) Electrochim Acta 37:1873
2. Tilak BV, Tari K, Hoover CL (1988) J Electrochem Soc 135:1386
3. Cornell A, Simonsson D (1993) J Electrochem Soc 140:3123
4. Lindbergh G, Simonsson D (1990) J Electrochem Soc 137:3094
5. Lindbergh G, Simonsson D (1991) Electrochim Acta 36:1985
6. Ahlberg Tidblad A, Lindbergh G (1991) Electrochim Acta 36:1605
7. Schumacher JW, Bradley R, Leder A, Takei N (1999) CEH product review, The chemical economics handbook-SRI international
8. Coleman JE (1981) In: Alkire R, Beck T (eds) Tutorial lectures in electrochemical engineering and technology, vol 77. American institute of chemical engineering symposium series no. 204, Institute of Chemical Engineers, New York, p 244
9. Andolfatto F, Joubert P, Duboeuf G (2004) FR 2852973
10. Guay D, Roue L, Schulz R, Bonneau M-E (2006) CA 2492128
11. Chow N, Socol J, Oehr K, Remple G (2006) WO 2006039804
12. Krstajic N, Jovic V, Martelli GN (2007) WO 2007063081
13. Jackson JR, Zhao M (2005) US 2005011753
14. Håkansson B, Fontes E, Herlitz F, Lindstrand V (2004) US 2004124094
15. Cornell A, Håkansson B, Lindbergh G (2003) Electrochim Acta 48:473
16. Nylén L, Cornell A (2006) J Electrochem Soc 153:D14
17. Coleman JE and Tilak BV (1995) In: McKetta JJ (ed) Encyclopedia of chemical processing and design. Marcel Dekker, Inc. N.Y., p 126
18. Tilak BV, Chen C-P (1999) In: Burney HS, Furuya N, Hine F, Ota KI (eds) Chlor-alkali and chlorate technology, PV 99–21. The electrochemical society proceedings series, Pennington, NJ, p 8
19. Ibl N, Vogt H (1981) In: Bockris JO′M, Conway BE, Yeager E, White RE (eds) Comprehensive treatise of electrochemistry, vol 2. Plenum Press, New York, p 167
20. Jaksic MM (1974) J Electrochem Soc 121:70
21. Hammar L, Wranglén G (1964) Electrochim Acta 9:1
22. Wulff J, Cornell A (2007) J Appl Electrochem 37:181
23. Hardee KL, Mitchell LK (1989) J Electrochem Soc 136:3314
24. Eberil VI, Fedotova NS, Novikov EA, Mazanko AF (2000) Elektrokhimiya 36:1463
25. Eberil VI, Fedotova NS, Novikov EA (1997) Elektrokhimiya 33:610
26. Elina LM, Gitneva VM, Bystrov VI, Shmygul NM (1974) Elektrokhimiya 10:68
27. Cornell A, Håkansson B, Lindbergh G (2003) J Electrochem Soc 150:D6
28. Jaksic MM, Nikolic BZ, Karanovic DM, Milovanovic CR (1969) J Electrochem Soc 116:394
29. YuV Dobrov, Elina LM (1967) Zashch Met 3:618
30. Nylén L, Behm M, Cornell A, Lindbergh G (2007) Electrochim Acta 52:4513
31. Albery J (1975) Electrode kinetics. Clarendon Press, Oxford, p 125
32. Hurlen T, Gunvaldsen S, Blaker F (1984) Electrochim Acta 29:1163
33. Ahlberg Tidblad A, Mårtensson J (1997) Electrochim Acta 42:389
34. Vračar LJ, Dražić DM (1992) J Electroanal Chem 339:269
35. Byrne P, Fontes E, Parhammar O, Lindbergh G (2001) J Electrochem Soc 148:D125
36. Koryta J, Dvorák J (1987) Principles of electrochemistry. Wiley, Great Britain, pp 264–276
37. Tamm J, Tamm L, Vares P (2000) Elektrokhimiya 36:1327
38. Jin S, Van Neste A, Ghali E, Boily S, Schultz R (1997) J Electrochem Soc 144:4272